iScience

CellPress
OPEN ACCESS

Article

Autocrine and paracrine effects of MDK promote lymph node metastasis of cervical squamous cell carcinoma

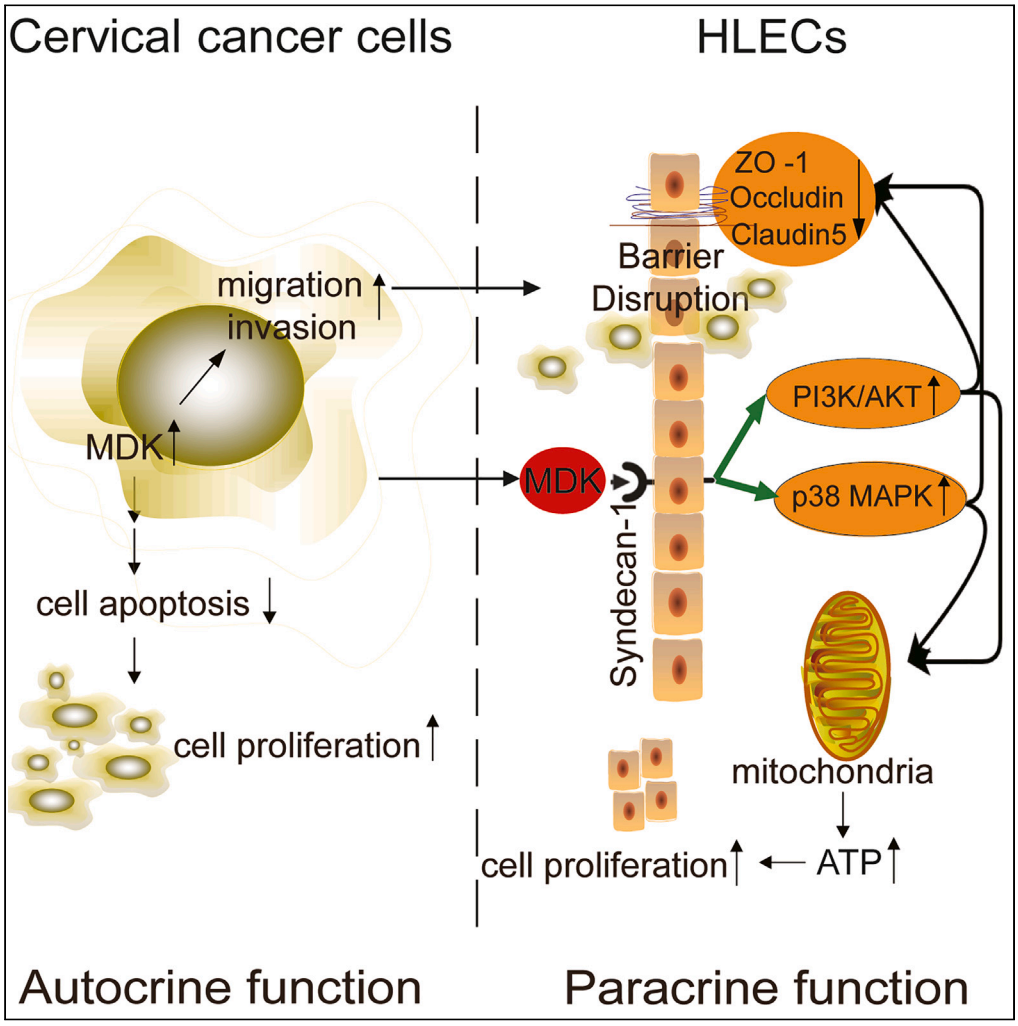

He Fei, Tong Chen, Hua Jiang

chentong@fudan.edu.cn (T.C.)
jianghua@fudan.edu.cn (H.J.)

Highlights

MDK is significantly correlated with LNM in CSCC

MDK regulates CSCC LNM from both autocrine and paracrine aspects

s-MDK combined with s-SCCA can improve the diagnostic accuracy of CSCC LNM

Fei et al., iScience 27, 110077
July 19, 2024
https://doi.org/10.1016/j.isci.2024.110077

iScience

CellPress
OPEN ACCESS

Article

Autocrine and paracrine effects of MDK promote lymph node metastasis of cervical squamous cell carcinoma

He Fei,[1] Tong Chen,[2,*] and Hua Jiang[3,4,5,*]

SUMMARY

Lymph node metastasis (LNM) is the main metastatic pathway of cervical cancer, which is closely related to 5-year survival rate of cervical squamous cell carcinoma (CSCC), yet the underlying mechanism remains unconfirmed. In this study, we show that midkine (MDK) was highly expressed in CSCC and overexpression of MDK was associated with CSCC LNM. Functional investigations demonstrated that MDK promoted LNM by enhancing proliferation, migration and invasion capacity of cervical cancer cells, facilitating lymphangiogenesis and down-regulating the expression of tight junction proteins of human lymphatic endothelial cells (HLECs). MDK exerted these biological effects by interacting with Syndecan-1 and activating PI3K/AKT and p38 MAPK pathways. A retrospective study showed that s-MDK was related to LNM. s-MDK combined with serum-squamous cell carcinoma antigen(s-SCCA) improved the diagnostic accuracy of CSCC LNM. These findings established a new mechanism of LNM and highlighted MDK as a candidate tumor biomarker and therapeutic target in CSCC.

INTRODUCTION

Cervical cancer is the fourth most common cancer in women worldwide[1] and still one of the top five malignant tumors leading female deaths.[2] Lymph node metastasis (LNM) is the major spreading route of cervical cancer. In 2018, the International Federation of Gynecology and Obstetrics (FIGO) included the LNM status in updated staging classification of cervical cancer,[3] as LNM is one of the most important clinical parameters in treatment determination. Current clinical guidelines recommend radical hysterectomy plus systematic pelvic lymphadenectomy as standard surgical procedure for early cervical cancer (IA-IIA), except for stage IA1.[3] However, a considerable part of patients without LNM have unnecessary systematic pelvic lymphadenectomy.[4] Associated irreversible damage seriously affect the postoperative life quality of patients.[5] Therefore, accurate assessment of LNM status is critical to treatment decisions for early cervical cancer.

Preoperative assessment for LNM usually employs imaging analysis (CT, MRI and PET),[6,7]which has a high false negative rate and low positive predictive value for LNM.[8] Squamous cell carcinoma antigen (SCCA) is the most extensive and reliable tumor marker used in assisted diagnosis of cervical squamous cell carcinoma (CSCC).[9] However, the diagnostic accuracy of s-SCCA for LNM was unsatisfactory.[10] Thus it's urgently needed to find some tumor markers closely related to LNM to assist in the assessment of CSCC LNM.

Midkine (MDK) is a promising tumor marker.[11] In recent years, studies have found that MDK are highly expressed in a variety of malignant tumors.[12] Serum-MDK(s-MDK) combined with other traditional tumor markers (CEA+ CA199/AFP) can improve the positive detection rate of early gastric cancer[13] and hepatocellular cancer.[14] Most of the researches on MDK and malignancy have focused on MDK's regulation of cell proliferation, apoptosis, survival, migration and invasion, vascular formation.[15,16] LNM is a complex process, the exact mechanisms have recently been the subject of intense interest.[17] Olmeda et al. reported that MDK promoted lymphangiogenesis and was associated with LNM in melanoma.[18] In endometrial carcinoma , preoperative s-MDK levels are significantly correlated with prognosis and the presence of LNM.[19] Hence, MDK may be involved in the LNM of malignant tumors and is a potentially useful tumor biomarker for LNM.

Studies have shown that the expression of MDK in cervical cancer tissues are significantly higher than that in normal cervical tissues.[20] However, whether MDK regulates CSCC LNM, the related molecular mechanism and its clinical diagnostic value are still unclear. Therefore, this study investigated the related effects and mechanisms of MDK on LNM of CSCC, and analyzed the clinical value of MDK in evaluating CSCC LNM.

[1]Department of Gynecology, The Fifth People's Hospital of Shanghai, Fudan University, Shanghai 200240, China
[2]Department of Hematology, Huashan Hospital, Fudan University, Shanghai 200040, China
[3]Department of Gynecology, Obstetrics & Gynecology Hospital, Fudan University, Shanghai 200011, China
[4]Shanghai Key Laboratory of Female Reproductive Endocrine Related Diseases, Shanghai 200011, China
[5]Lead contact
*Correspondence: chentong@fudan.edu.cn (T.C.), jianghua@fudan.edu.cn (H.J.)
https://doi.org/10.1016/j.isci.2024.110077

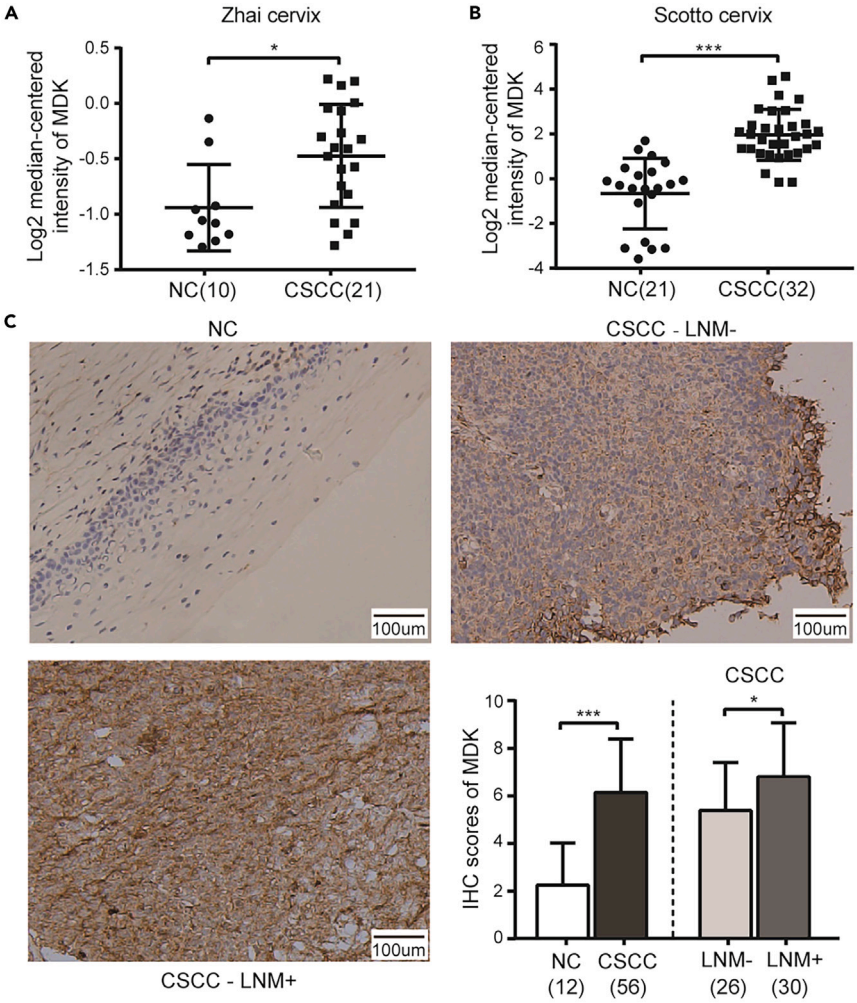

Figure 1. MDK is upregulated in CSCC and correlated with LNM

(A) The expression of MDK mRNA in CSCC tissue and human cervical squamous epithelium from Zhai cervix databases in Oncomine. The difference of MDK mRNA expression between groups was analyzed; the ordinate is the median of log2 of MDK mRNA value.

(B) The expression of MDK mRNA in CSCC tissue and human cervical squamous epithelium from Scotto cervix databases in Oncomine. The difference of MDK mRNA expression between groups was analyzed; the ordinate is the median of log2 of MDK mRNA value.

(C) The typical picture of IHC staining of MDK protein in normal cervical tissue and cancer tissue of CSCC-LNM+/CSCC-LNM-; Scale bar = 100 μm. The differences of IHC scores of MDK between groups (NC vs. CSCC and CSCC-LNM+ vs. CSCC-LNM-) were analyzed. The data represented the median with 95% CI. *$p < 0.05$, ***$p < 0.001$.

RESULTS

The expression of MDK is upregulated in CSCC and correlated with LNM

MDK mRNA expression profiles were extracted from two datasets in Oncomine database: Zhai Cervix and Scotto Cervix. Zhai cervix database included 10 cases of cervical squamous cell epithelial tissue and 21 cases of CSCC. Scotto cervix database contained 24 cases of cervical squamous epithelium and 32 cases of CSCC. Log2 of MDK RNA value was statistically analyzed. It was shown that the level of MDK mRNA in CSCC tissues (CSCC group) was significantly higher than that in normal cervical epithelial tissue (NC group) (Zhai Cervix: $p = 0.0105$, Scotto Cervix: $p < 0.001$), and the results of two databases were consistent (Figures 1A and 1B). Immunohistochemistry (IHC) staining were performed on samples from 11 CSCC and 12 NC, the results showed a similar pattern of elevated MDK expression in CSCC group compared with NC group ($p < 0.01$) (Figure 1C; Table S1); These results suggested that MDK was highly expressed in CSCC tissues.

Meanwhile, we noticed an interesting phenomenon that the expression of MDK in 2 CSCC-LNM+ was significantly higher than that of CSCC-LNM- (Figure 1C). To explore whether MDK was associated with CSCC LNM, the sample size was expanded according to the pre-experimental test results. The minimum sample size calculated byPASS software was 17. Ultimately, 30 CSCC-LNM+ and 26 CSCC-LNM- were included. MDK level was significantly elevated in CSCC tissues ($n = 56$) compared with normal cervical tissues($n = 12$) ($p < 0.001$).

Table 1. Relationship between MDK expression and tumor characteristics in 56 CSCC samples

Variant	No. (%)	MDK		*p*-value	Odds Ratio (95% CI)
		–	+		
Age				0.762	0.041(-0.223–0.318)
< median = 51year	26(46.43%)	7(26.92%)	19(73.08%)		
≥ median = 51year	30(53.57%)	6(20%)	24(80%)		
FIGO stage				0.02	0.309(0.015–0.576)
Early stage (I-IIA)	18(32.14%)	8(44.44%)	10(55.56%)		
Advanced stage (IIB-III)	38(67.86%)	5(13.16%)	33(86.84%)		
Lymph node metastasis				0.031	0.289(0.019–0.524)
Yes	30(53.57%)	3(10%)	27(90%)		
No	26(46.43%)	10(38.46%)	16(61.54%)		
Extent of myometrial invasion				0.036	0.281(0.054–0.569)
<1/3	7(12.5%)	4(57.14%)	3(42.86%)		
≥2/3	49(87.5%)	9(18.37%)	40(81.63%)		
Parauterine infiltration				0.757	0.042(-0.250–0.287)
Yes	22(39.29%)	7(31.82%)	15(68.18%)		
No	34(60.71%)	6(17.65%)	26(82.35)		
Tumor size (largest diameter)				0.034	0.283(0.040–0.505)
<4cm	14(25%)	6(42.86%)	8(57.14%)		
≥4cm	42(75%)				
1 line	23(41.07%)	5(21.74%)	18(78.26)		
2-3 lines	19(33.93%)	2(10.52%)	17(89.48%)		
Vascular Invasion				0.592	0.073(-0.184–0.332)
Yes	43(76.79%)	9(20.93%)	34(79.07%)		
No	13(23.21%)	4(30.77%)	9(69.23%)		

The expression of MDK in CSCC-LNM+ group was significantly higher than that of CSCC-LNM-group (Figure 1C) and was significantly associated with LNM (Table 1). MDK expression was also significantly correlated with FIGO stage, tumor size and muscle invasion, but not with patient's age, parauterine infiltration and vascular invasion (Table 1).

All these findings demonstrate that MDK is highly expressed in CSCC tissues and is significantly correlated with LNM.

MDK promotes growth and tumorigenicity of cervical cancer cells

To test whether MDK plays a role in the pathophysiology of CSCC, we first examined MDK expression in five cervical cancer cell lines (C33a, Caski, HeLa, MS751, Siha). By analyses of IHC and RT-PCR, we found that MDK expression was highest in C33a cells, but lowest in MS751 cells (Figures 2A and S1A). In conditioned media of corresponding cell lines, Enzyme linked immunosorbent assay (ELISA) based quantification detection of MDK showed consistent results (Figure 2B).

Then loss-of-function studies were performed in C33a cells while gain-of function studies in MS751 cells, to manipulate the endogenous levels of MDK. For loss-of-function studies, 3 shRNAs were tested. Of those, Real-time PCR (RT-PCR), IHC and ELISA identified shMDK (1) and (3) as potent blockers of MDK expression and secretion (Figures 2C, 2D, and S1B). For gain-of function studies, MDK is effectively overexpressed in MS751 cells (Figures 2E, 2F, and S1B).

Due to LNM burden positively correlates with primary tumor size,[21] the effect of MDK on cell proliferation and tumor growth were determined. Depletion of MDK resulted in impaired cell proliferation and colony formation capacity in C33a cells while after MDK was overexpressed in MS751 cells, cell proliferation and colony formation capacity were enhanced significantly (Figures 2G–2J).

To further illustrate the mechanism underlying the proliferative effect of MDK, the cellular capability of apoptosis resistance was determined. Analyses of annexin V/7-AAD apoptosis and apoptosis-related protein active-Caspase3 assays were performed after apoptosis was induced by 0.5% H_2O_2 culture. After silencing of MDK, the total apoptotic rate and the expression of active-Caspase3 of C33a cells was significantly increased (Figures 2K–2M). Conversely, after overexpression MDK, the total cell apoptosis rate and the expression of active-Caspase3 of MS751 cells decreased (Figures 2L and S1C). A serum free media was applied to the cell culture system for 48h, then the expression of Bcl2 and Bax were investigated by WB. The overexpression of MDK in MS751 cells resulted in a decrease of apoptosis-promoting protein Bax, while antiapoptotic protein Bcl2 was elevated (Figure 2N).

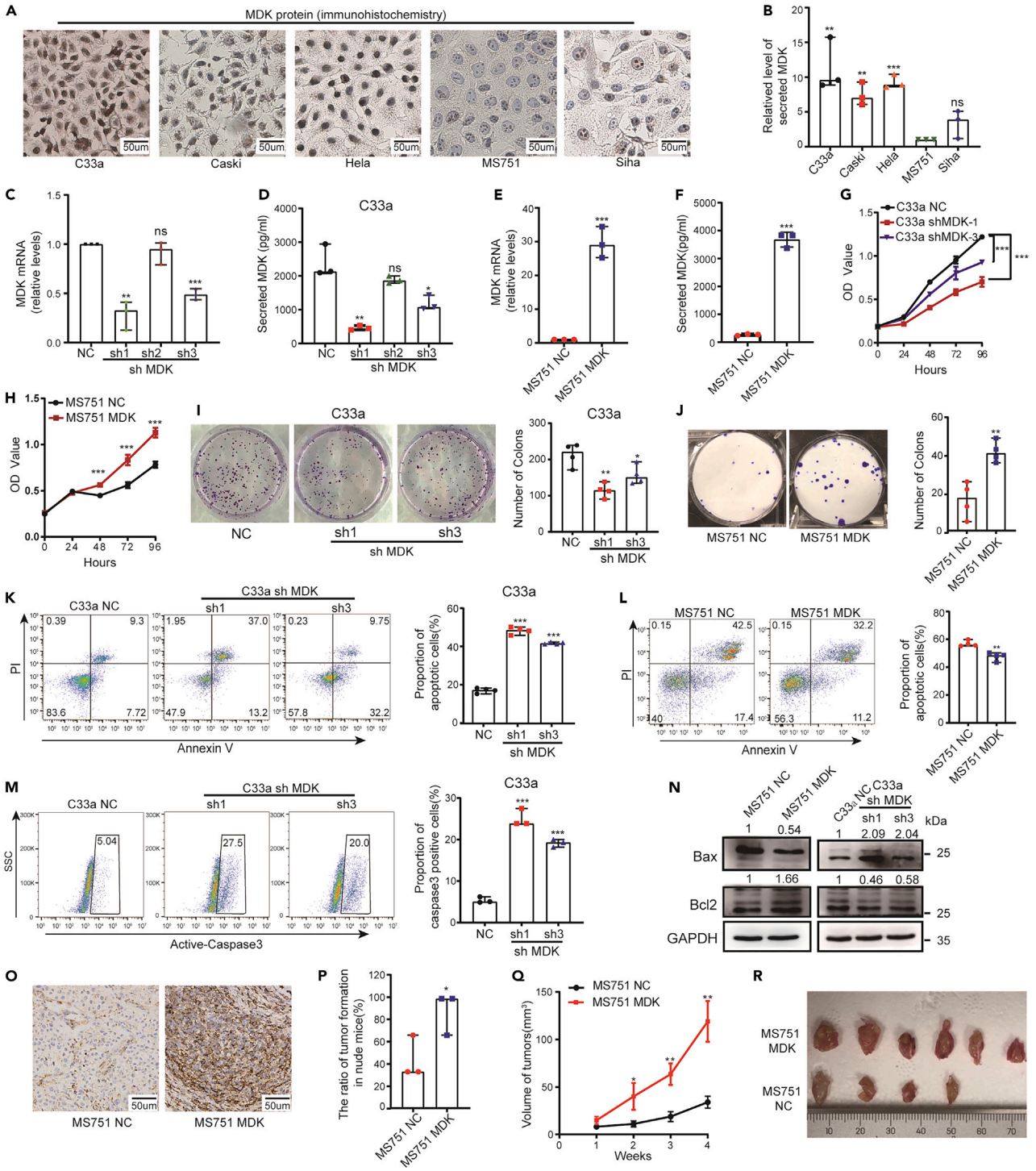

Figure 2. MDK promotes growth and tumorigenicity of cervical cancer cells

(A) IHC analysis of MDK expression in five cervical cancer cell lines. Scale bar = 50 μm.

(B) The level of MDK protein secreted in the supernatant of five cervical cancer cells was detected by ELISA and normalized to the levels measured in the MS751 cell line (=1).

(C) The RT-PCR results showed the efficiencies of knockdown of MDK in C33a cells.

(D) The ELISA results showed the efficiencies of knockdown of MDK in C33a cells.

(E) The RT-PCR results showed the efficiencies of overexpress of MDK in MS751 cells.

Figure 2. *Continued*

(F) The ELISA results showed the efficiencies of overexpress of MDK in MS751 cells.

(G) CCK8 experiment detected the proliferation ability of C33a shMDK-1, C33a shMDK-3 and C33a NC cells.

(H) CCK8 experiment detected the proliferation ability of MS751 MDK and MS751 NC cells.

(I) Colony formation assay of C33a shMDK-1, C33a shMDK-3 and C33a NC cells (left panel). The colony numbers of three groups were compared (right panel).

(J) Colony formation assay of MS751 MDK and MS751 NC cells (left panel). The colony numbers of two groups were compared (right panel).

(K) FACS analysis of Annexin V in C33a shMDK-1, C33a shMDK-3 and C33a NC cells. Data were showed as dot plot (left panel) and grouped percentage of apoptotic cells (right panel).

(L) FACS analysis of Annexin V in MS751 MDK and MS751 NC cells. Data were showed as dot plot (left panel) and grouped percentage of apoptotic cells (right panel).

(M) FACS analysis of active caspase-3 in C33a shMDK-1, C33a shMDK-3 and C33a NC cells.

(N) Expression of Bax and Bcl2 was analyzed by WB. MS751 MDK and MS751 NC cells (left panel), C33a shMDK-1, C33a shMDK-3 and C33a NC cells (right panel).

(O) Expression of MDK in transplanted tumor of foot pad was validated by IHC analysis. Scale bar = 50 μm.

(P) The ratio of tumor formation in MS751 NC group and MS751 MDK group.

(Q) Footpad transplanted tumor growth curves of mice in MS751 NC group and MS751 MDK group are depicted.

(R) The representative pictures of dissected tumors from nude mice transplanted with stable MS751 NC and MS751 MDK cells. The data represent the median with 95% CI. Each experiment was independently repeated at least three times. *$p < 0.05$, **$p < 0.01$, ***$p < 0.001$.

In vivo, the tumor formation rate and tumor growth rate were observed when constructing hindfoot lymphatic drainage model using MS751 MDK/MS751 NC cells. MDK expression in dissected tumors was validated by IHC (Figure 2O). Consequently, MS751 MDK cells show an increased ability to form solid tumors in mice (MS751 MDK vs. MS751 NC: 88.89% ± 11.11% vs. 44.44% ± 11.11%, $p = 0.047$) (Figure 2P). The growth rate of the footpad transplanted tumors of MS751 MDK group was significantly faster than that of MS751 NC group (Figure 2Q); On the 28th day, the footpad transplanted tumor volume in MS751 MDK group was significantly larger than that of MS751 NC group (116.6 ± 9.309mm^3 vs. 62.52 ± 10.8mm^3, $p = 0.002$) (Figures 2R and S1D).

Together, these results demonstrate that MDK plays an important oncogenic role in cervical cancer *in vitro* and *in vivo*.

MDK promotes cervical cancer metastasis

To demonstrate the potential effects of MDK for promoting metastasis in cervical cancer, Transwell assays were performed. The results indicated that MDK overexpression increased the invasion and migration ability of MS751 cells and resulted in upregulated expression of MMP9 and MMP2 (Figures 3A and 3C), whereas MDK knockdown significantly decreased the invasion ability of C33a cells and downregulated expression of MMP9 and MMP2 (Figures 3B and 3C).

Cervical cancer cell-derived MDK promotes LNM *in vitro* and *in vivo*

Since lymphangiogenesis and lymphatic barrier function are crucial for tumor LNM, the effects of MDK on the proliferation ability, sprouting, tube formation and the expression of tight junction proteins (TJPs) (ZO-1, Claudin5, and occludin) of Human lymphatic endothelial cells (HLECs) were investigated.

Compared with control group, the culture supernatants of MDK-overexpressing cells significantly promoted the ability of proliferation, sprouting and tube formation of HLECs (Figures 3D–3F). In contrast, MDK knockdown abolished these effects of C33a cell (Figures 3G, 3H, and S2A). Thus, we conclude that cervical cancer cell-derived MDK promotes lymphangiogenesis. The conditioned medium of MS751 MDK cells significantly down-regulated the expression of ZO-1, Claudin5 and occluding (Figures 3I, 3J, and S2B). However, after MDK silencing, the expression of TJPs was increased (Figures 3I, 3J, and S2C).

The hindfoot lymphatic drainage model was constructed. On the 28th day, the mice were sacrificed and dissected for observation. To label lymph node, 20 μL of 155kDa TRITC dextran was injected intradermally at the lateral tail base on the tumor side 5 min before execution. The visible enlarged lymph nodes in MS751 MDK group were significantly more than those in MS751 NC group (Figure 3K). The enlarged lymph nodes were observed under confocal microscope or frozen section. The detection of green fluorescence of tumor cells in lymph nodes represents the occurrence of LNM (Figures S2D and S2E). Among 7 MS751 NC mice and 14 MS751 MDK mice that formed tumors, the number of lymph nodes with metastasis per mouse in MS751 NC group was significantly lower than that in MS751 MDK group ($p = 0.02$) (Figure 3L). MS751 MDK group had more Lyve-1-positive lymphatic vessels, and more tumor cells infiltrated into lymphatic vessels (Figures 3M and 3N).

MDK interacts with Syndecan-1 and activates PI3K/AKT and p38 MAPK pathways to promote lymphangiogenesis and down-regulate the expression of TJPs

The effects of recombinant human MDK protein on the related functions of HLECs were further studied. Compared with the control group, 25ng/mL-100 ng/ml MDK protein had a significant promoting effect on proliferation of HLECs at 24h and 48h (Figures 4A, 4B, and S3A). Further narrowing the range of MDK concentration, 12.5 ng/ml MDK showed no significant promoting effect at 24h, while 25 ng/ml MDK showed significant promoting effect on HLECs ($p = 0.003$) (Figure 4C). Therefore, the optimal concentration for subsequent action was determined to be 25 ng/ml. MDK protein down-regulated the TJPs expression of HLECs in a concentration-dependent manner (Figure 4D).

HLECs were incubated in conditioned medium of MS751 MDK/MS751 NC cells for 24h, then collected for transcriptomic sequencing. Three independent replicates were performed for each sample. 22692 genes were detected in total, including 117 up-regulated genes

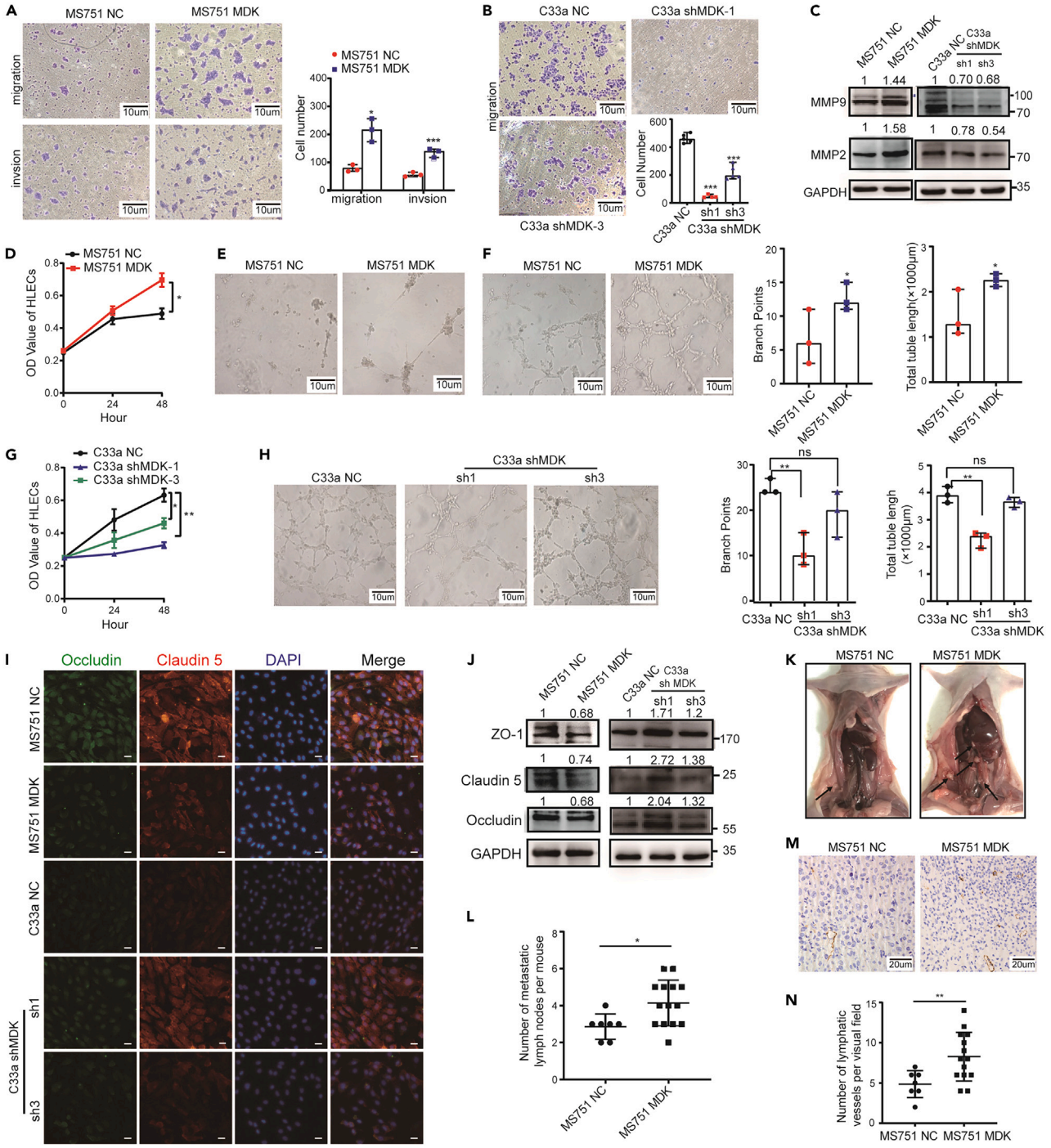

Figure 3. Cervical cancer cell-derived MDK promotes LNM in vitro and in vivo

(A) Transwell assay (migration and invasion) of MS751 NC and MS751 MDK cells. Scale bar = 10 μm.

(B) Transwell assay(migration) of C33a shMDK-1, C33a shMDK-3 and C33a NC cells. Scale bar = 10 μm.

(C) Expression of MMP2 and MMP9 was analyzed by WB. MS751 MDK and MS751 NC cells (left panel), C33a shMDK-1, C33a shMDK-3 and C33a NC cells (right panel).

(D) CCK8 experiment detected the proliferation ability of HLECs cultured by conditioned medium of MS751 MDK/MS751 NC cells.

(E) Typical diagram of sprouting of HLECs pretreated with conditioned medium of MS751 MDK/MS751 NC cells. Scale bar = 10 μm.

(F) HLECs were pretreated with conditioned medium of MS751 MDK/MS751 NC cells to investigate the effects of MDK on the tube formation of HLECs. Representatives are shown (left panel). Total branch points and total tuber length were calculated (right panel). Scale bar = 10 μm.

Figure 3. *Continued*

(G) CCK8 experiment detected the proliferation ability of HLECs cultured by conditioned medium of C33a shMDK-1/C33a shMDK-3/C33a NC cells.

(H) HLECs were pretreated with conditioned medium of C33a shMDK-1/C33a shMDK-3/C33a NC cells to investigate the effects of MDK on the tube formation of HLECs. Representatives are shown (left panel). Total branch points and total tuber length were calculated (right panel). Scale bar = 10 μm.

(I) Immunofluorescence staining of Occludin (blue), Claudin5 (red) and DAPI (green) in HLECs cultured by conditioned medium. Scale bar = 100 μm.

(J) The expressions of ZO-1, Claudin5 and Occludin in HLECs cultured by conditioned medium were analyzed by WB.

(K) Typical images of gross anatomy of hindfoot lymphatic drainage model constructed by MS751 MDK/MS751 NC cells; Black arrows: the visible enlarged lymph nodes.

(L) The number of metastatic lymph nodes in MS751 NC group and MS751 MDK group were compared.

(M) Expression of LYVE-1 in transplanted tumor of foot pad was validated by IHC analysis. Scale bar = 20 μm.

(N) The number of lymphatic vessels per visual field in MS751 NC group and MS751 MDK group were compared. The data represent the median with 95%CI. Each experiment was independently repeated at least three times. *$p < 0.05$, **$p < 0.01$, ***$p < 0.001$.

and 34 down-regulated genes (Data are not showed). KEGG pathway enrichment was performed for the up-regulated genes, and PI3K/AKT pathway was among the enriched signaling pathways (Figure 4E). The PI3K/AKT and p38 MAPK signaling pathway have been reported to be involved in regulating proliferation,[22] permeability and tight connection[23] of cells. Therefore, we verified the regulatory effect of MDK on PI3K/AKT and p38 MAPK signaling pathway.

Phosphorylation of AKT and p38 MAPK (*p*-AKT and p-p38 MAPK) were activated after HLECs was stimulated by MDK (25 ng/ml) at 10mins and 20mins (Figure 4F). *p*-AKT and p-p38 MAPK were activated in a concentration-dependent manner at 10mins (Figure 4G). Cervical cancer cell-derived MDK significantly activated *p*-AKT and p-p38 MAPK, while after MDK silencing, phosphorylation of AKT and p38 MAPK decreased compared with NC group (Figure S3B).

GO function enrichment of the differential genes showed that the differential genes were mainly concentrated in the response to hypoxia (Figure S3C). According to literature review, mitochondrial function is involved in the cell's response to hypoxia.[24] Mitochondria are the main organelles that provide energy for cell proliferation.[25] After MDK applied to HLECs for 24h, we detected the change of HLECs membrane potential. Compared with control group, the green fluorescence of HLECs in 25 ng/ml MDK group was significantly weakened, and the ratio of red to green fluorescence significantly increased, which meant mitochondrial function was enhanced ($p = 0.0464$) (Figure 4H). 25 ng/ml MDK significantly increased the ATP production capacity of HLECs ($p < 0.001$) (Figure 4I). It has been reported that PI3K/AKT pathway maybe involved in regulating mitochondrial function.[26,27]

We further confirmed whether MDK down-regulated TJPs expression by activating the PI3K/AKT and P38 MAPK pathways. PI3K inhibitor (LY294002) or Akt inhibitor (MK2206) or p38 MAPK inhibitor (SB203580) were used to pretreat HLECs for 1h, then MDK (25 ng/ml) stimulated HLECs for 24h. LY294002 and MK2206 attenuated MDK's down-regulation of TJPs in HLECs and prevent phosphorylation of AKT induced by MDK (Figures 4J and 4K). SB203580 also reversed the down-regulation of TJPs by MDK and prevent phosphorylation of p38 MAPK (Figure 4L). Hence, PI3K/AKT and p38 MAPK signaling pathways are involved in MDK-mediated down-regulation of TJPs expression.

Syndecan-1 is one of the receptors for MDK[28] and has been reported to regulate the expression of TJPs (ZO-1, occludin).[29] We found that after siRNA interference with Syndecan-1 expression (Figure S3D), MDK's effect on TJPs down-regulation was weakened (Figures 4M and 4N), phosphorylation of AKT and p38 MAPK was partially inhibited (Figure 4O). Therefore, we concluded that MDK regulated TJPs expression through its interaction with Syndecan-1.

Clinical value of s-MDK in evaluating CSCC LNM

The median s-MDK level of CSCC was 492.792 pg/ml, which was significantly higher than that in healthy control subjects (NC group) at 242.184 pg/ml ($p < 0.001$) (Figure 5A). Taking 242.184 pg/ml as the reference value, the prevalence of s-MDK hyperexpression in CSCC group was significantly higher than that in NC group (72.4% vs. 45.2%). The median s-MDK level of CSCC-LNM+ at 1392.058 pg/ml was significantly higher than that of CSCC-LNM-at 292.907 pg/ml ($p = 0.001$) (Figure 5B). To analyze the diagnostic power of s-MDK as biomarker for CSCC LNM, a receiver operation characteristic (ROC) curve was mapped out. The AUC was 0.758 ($p < 0.001$). There is a balanced relationship between sensitivity (72.7%) and specificity (83.8%) when the cut-off value is set at 641.793 pg/ml (Figure 5C). Then 640 pg/ml was chosen as the cut-off value. s-MDK was related to LNM ($p < 0.001$), FIGO stage ($p < 0.001$), tumor size ($p = 0.004$), muscle invasion ($p = 0.043$) and vascular invasion ($p = 0.014$), but not related to the patient's age (Table 2).

As the diagnostic accuracy of s-MDK for CSCC LNM is general, we try to combine s-MDK and SCCA to assess CSCC LNM. The expression of s-SCCA was detected. As the serum samples of 5 LNM-patients were used up in s-MDK test and 2 LNM-patients were invalidated (value not shown), 64 CSCC-LNM+ and 63 CSCC-LNM-were included. The median s-SCCA level in CSCC-LNM+ group was 0.886 ng/ml, which was significantly higher than the 0.241 ng/ml in CSCC-LNM-group ($p < 0.001$) (Figure 5D). The ROC curve of s-SCCA level for CSCC LNM was mapped out, AUC was 0.716($p<0.05$). There was a balanced relationship between sensitivity(53.8%) and specificity (88.7%) when the cut-off value was set at 0.795 ng/ml (Figure 5E).

The correlation between s-MDK and s-SCCA were analyzed. The Pearson correlation coefficient was −0.027($p = 0.764$) (Datas are not shown), indicating that s-MDK and s-SCCA are independent of each other. Therefore, the ROC curve of s-MDK combined with s-SCCA for CSCC LNM were mapped up. The AUC is 0.829, 95%CI 0.754–0.903($p<0.001$) (Figure 5F). Therefore, it is concluded that s-MDK combined with s-SCCA improved the diagnostic accuracy for CSCC LNM.

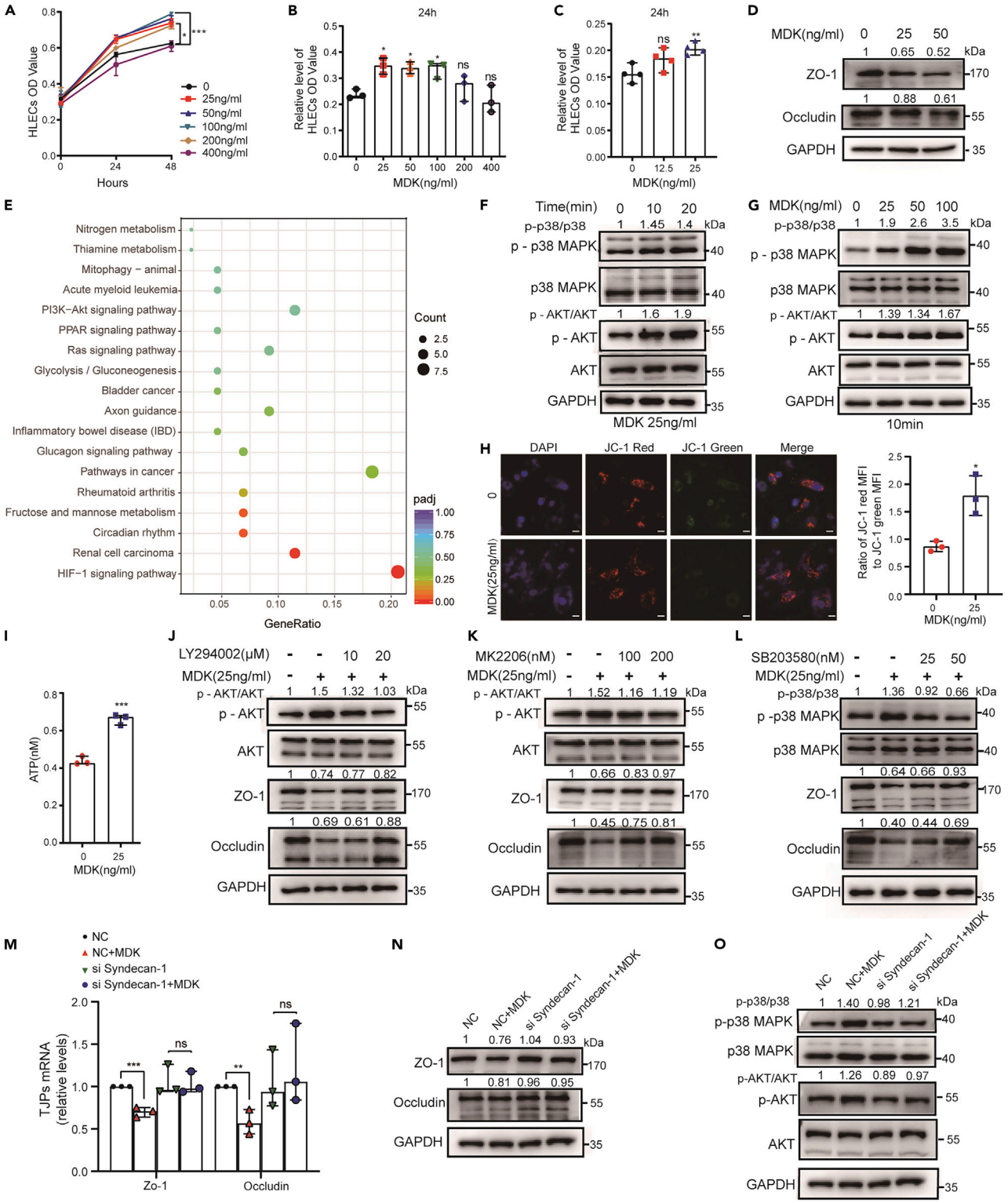

Figure 4. MDK interacts with Syndecan-1 and activates PI3K/AKT and p38MAPK pathways to promote lymphangiogenesis and down-regulate the expression of TJPs

(A) CCK8 assay was used to detect the effects of different concentrations of recombinant human MDK protein(0-400 ng/ml) on the proliferation of HLECs.

(B) The effects of different concentrations of recombinant human MDK protein(0-400 ng/ml) on the proliferation of HLECs for 24h.

Figure 4. *Continued*

(C) The effects of recombinant human MDK protein (0, 12.5 ng/ml, 25 ng/ml) on the proliferation of HLECs for 24h.

(D) The expressions of ZO-1and Occludin in HLECs treated by MDK protein (0, 25 ng/ml, 50 ng/ml) were analyzed by WB.

(E) Point diagram of KEGG pathway enrichment of upregulated genes detected by transcriptomic sequencing, which performed on HLECs pretreated with conditioned medium of MS751 MDK/MS751 NC cells.

(F) WB was used to detect the phosphorylation of AKT and p38 MAPK at different time points of HLECs treated with 25 ng/mL MDK protein.

(G) WB was used to detect the phosphorylation of AKT and p38 MAPK when HLECs were treated with MDK protein (0, 25 ng/ml,50 ng/ml,100 ng/ml) for 10min.

(H) Mitochondrial membrane potential as the ratio of JC-1 red to JC-1 green was detected by immunofluorescence (left panel), scale bar = 200μm.The ratio of red to green fluorescence was analyzed by ImageJ (right panel).

(I) ATP production of HLECs treated with MDK protein (0.25 ng/ml) was detected by ATP detection kit.

(J) The expressions of ZO-1, Occludin, AKT and p - AKT in HLECs pretreated by 25 ng/ml MDK protein and/or PI3K inhibitor (LY294002) were analyzed by WB.

(K) The expressions of ZO-1, Occludin, AKT and p - AKT in HLECs pretreated by 25 ng/ml MDK protein and/or AKT inhibitor (MK2206) were analyzed by WB.

(L) The expressions of ZO-1, Occludin, p38 MAPK and p - p38 MAPK in HLECs pretreated by 25 ng/ml MDK protein and/or p38 MAPK inhibitor (SB203580) were analyzed by WB.

(M) The RT-PCR results showed after siRNA interference with Syndecan-1 expression, MDK's effect on TJPs down-regulation.

(N) The expressions of ZO-1, Occludin in HLECs after siRNA interference with Syndecan-1 expression were analyzed by WB.

(O) The expressions of AKT, *p*-AKT, p38 MAPK and p - p38 MAPK in HLECs after siRNA interference with Syndecan-1 expression were analyzed by WB. The data represent the median with 95%CI. Each experiment was independently repeated at least three times. $*p < 0.05$, $**p < 0.01$, $***p < 0.001$.

DISCUSSION

The ability of tumor cells' LNM is not only related to the proliferation, motility and invasion ability of tumor cells, but also closely related to the influence on lymphangiogenesis and lymphatic barrier function.[30] This article clarifies the effects of MDK on cervical cancer LNM from two perspectives: (1) Autocrine function: MDK promoted the growth of cervical cancer and enhanced the migration and invasion ability of cervical cancer cells; (2) Paracrine function: MDK promoted lymphangiogenesis and impaired lymphatic barrier function.

In this study, MDK expression was elevated in CSCC group compared to NC group. Overexpression of MDK in CSCC may be caused by multiple factors, such as tumor-related inflammation or genetic mutations. Interferon(IFN-γ) exposure promotes MDK expression in cervical cancer cell line CaSki and drove cancer metastasis via STAT1.[31] Meanwhile, IFN-γ was upregulated in HPV-positive cases and was significantly increased with the disease severity in cervical lesions.[32] In gallbladder carcinoma, ErbB mutations upregulate MDK via PI3K/AKT.[33] In 2017, nature reported that ERBB3 was identified as a new significantly mutated gene in cervical cancer.[34] All these are speculations, and the specific molecular mechanism of MDK overexpression in CSCC needs further study.

Another founding was that the expression of MDK was related to LNM of CSCC. There have also been previous reports of associations between MDK and LNM in malignancies. In colorectal cancer, MDK expression levels were independently associated with LNM.[35] Melanoma patients with higher MDK expression in sentinel lymph nodes had significantly lower rates of disease-free survival.[18] All of these studies are consistent with our conclusions.

Abnormal expression of TJPs in HLECs can lead to reduced lymphatic barrier function,[36] increased permeability, and ultimately lead to lymphatic metastasis of tumor cells.[37] The signal pathways involved in regulating cell tight junctions mainly include PKC, Rho GTPase and PI3K/AKT.[38] Studies have shown that different stimulating factors activate PI3K/AKT pathway, which may have different regulatory effects on tight junctions. In human aortic endothelial cells, VEGF down-regulates the expression of Claudin-5 by activating PI3K/AKT/Snail2 pathway.[39] However, after brain trauma, fibroblast growth factor activates PI3K/AKT/Rac1 pathway and upregulates TJPs to maintain the integrity of the cerebrovascular barrier.[23] Our research showed that by interacting with Syndecan-1 and activating PI3K/AKT and p38 MAPK pathways, MDK down-regulated the expression of TJPs in HLECs, impaired the lymphatic barrier function, thereby promoted CSCC LNM.

It is worth noting that PI3K/AKT signaling pathway is closely related to mitochondrial function.[27] AKT was a regulator of both glycolytic and oxidative energy metabolism, which stimulated ATP production via glycolysis[26] as well as via OXPHOS.[40] With respect to bioenergetics, the β-subunit of ATP synthase was identified as an AKT interaction partner in mitochondrial,[27] which leads to increased ATP production. Our studies showed that MDK enhanced mitochondrial function. Therefore, we speculated that MDK enhanced mitochondrial function and stimulated ATP production by activating the PI3K/AKT signaling pathway, thereby promoting lymphangiogenesis.

Previous studies have shown that MDK combined with other tumor markers can improve diagnostic effectiveness. After MDK combined with AGR2 and CA125, the AUC increased from 0.734 to 0.988, which significantly improved the diagnostic efficacy of ovarian cancer.[41] In this study, after s-MDK combined with s-SCCA, the AUC increased from 0.758 to 0.829. However, the diagnostic accuracy was still not satisfactory. It may be related to the small sample size. In future studies, in addition to expanding the sample size, we can also try to include other tumor markers (such as CEA, CA125, cervical cancer-associated antigen TA-4) and imaging tests, explore the combined application to improve the diagnostic accuracy of CSCC LNM and benefit CSCC patients.

In conclusion, MDK as a promising biomarker for CSCC. Thus, our findings provide new insights into the mechanism of CSCC LNM and add a promising new biomarker for the assist assessment of CSCC LNM.

Limitations of the study

Although this study shows that s-MDK combined with s-SCCA can improve the diagnostic accuracy of CSCC LNM, the AUC value is relatively low, which may be related to the relatively small sample size included. In subsequent studies, the sample size can be expanded

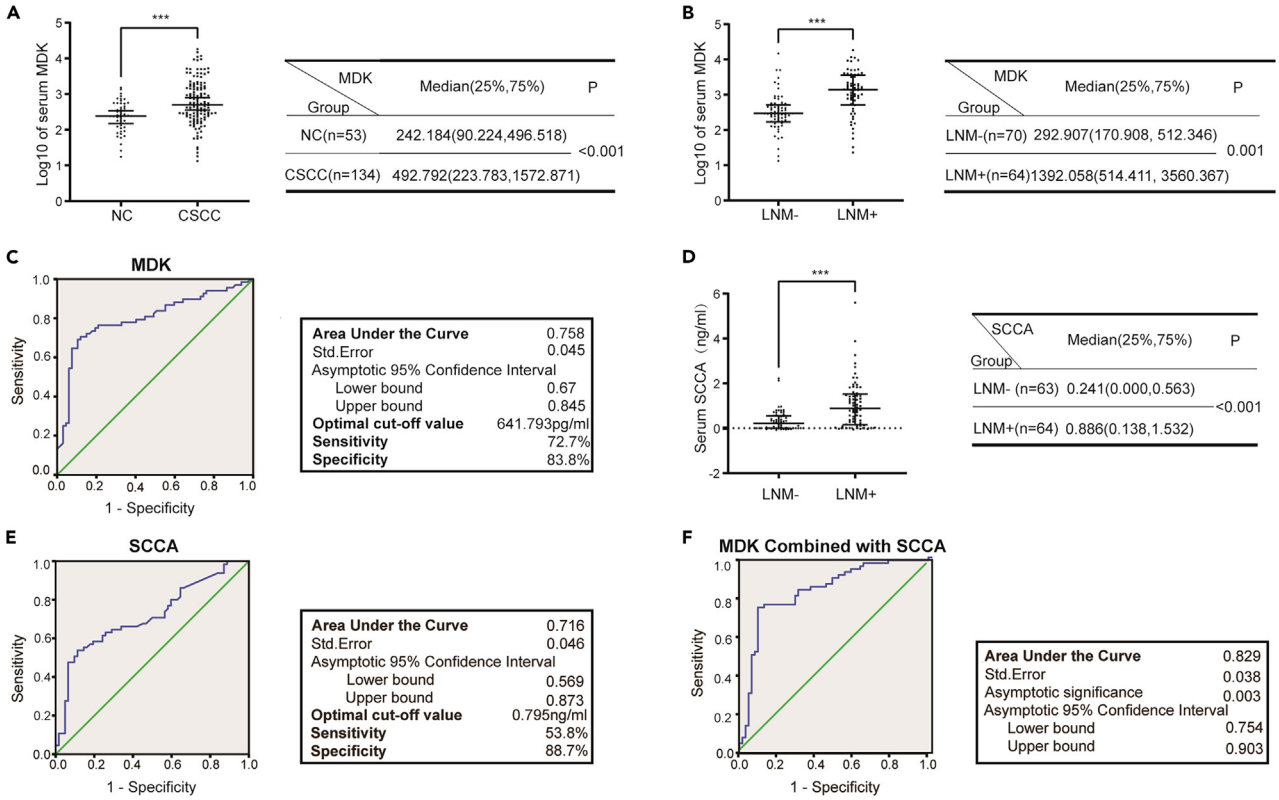

Figure 5. s-MDK combined with s-SCCA improves the diagnostic accuracy for CSCC LNM

(A) s-MDK level of CSCC group and NC group were tested by ELISA (left panel), the ordinate is the median of log10 of s-MDK value. The difference of s-MDK level between CSCC group and NC group was analyzed(right panel).

(B) s-MDK level of CSCC LNM+ group($n = 64$) and CSCC LNM-group($n = 70$) were tested by ELISA (left panel), the ordinate is the median of log10 of s-MDK value. The difference of s-MDK level between CSCC LNM+ group and CSCC LNM-group was analyzed(right panel).

(C) ROC curve of s-MDK level for diagnosis of CSCC LNM was mapped out.

(D) s-SCCA level of CSCC LNM+ group ($n = 64$) and CSCC LNM-group($n = 63$) were tested by ELISA (left panel). The difference of s-SCCA level between CSCC LNM+ group and CSCC LNM-group was analyzed (right panel).

(E) ROC curve of s-SCCA level for diagnosis of CSCC LNM was mapped out.

(F) ROC curve of s-MDK combined with s-SCCA level for diagnosis of CSCC LNM was mapped out. The data represent the median (25%,75%). $*p < 0.05$, $**p < 0.01$, $***p < 0.001$.

to further verify its clinical application value. It is also possible to try to include other tumor markers, such as CEA, CA125, and cervical cancer associated antigen TA-4, to analyze the diagnostic effectiveness of the combined diagnosis of multiple tumor markers. The combination of s-MDK and imaging can also be studied to explore whether the diagnostic accuracy can be improved to benefit patients with CSCC.

STAR★METHODS

Detailed methods are provided in the online version of this paper and include the following:

- KEY RESOURCES TABLE
- RESOURCE AVAILABILITY
  - Lead contact
  - Materials availability
  - Data and code availability
- EXPERIMENTAL MODEL AND STUDY PARTICIPANT DETAILS
  - Cell lines
  - Hindfoot lymphatic drainage model
  - Human studies
- METHOD DETAILS

Table 2. Association of s-MDK with tumor characteristics in 134 CSCC samples

		MDK (pg/mL)			
Variant	No. (%)	Low level (<640)	High level (≥640)	*p*-value	Odds Ratio(95% CI)
Age				0.488	0.784(0.393–1.562)
< median = 45years	75	40(53.33%)	35(46.67%)		
≥median = 45years	59	35(59.32%)	24(40.68%)		
FIGO分期				<0.001	8.545(3.789–19.273)
Early stage (I-IIA)	61	50(81.97%)	11(18.03%)		
Advanced stage (IIB-III)	73	25(34.25%)	48(65.75%)		
Lymph node metastasis				<0.001	9.474(4.282–20.959)
Yes	64	19(29.69%)	45(70.31%)		
No	70	56(80%)	14(20%)		
Extent of myometrial invasion				0.029	2.218(1.084–4.536)
<1/3	55	37(67.27%)	18(32.73%)		
≥2/3	79	38(48.10%)	41(51.9%)		
Tumor size (largest diameter)				0.001	3.860(1.726–8.633)
<4cm	97	63(64.95%)	34(35.05%)		
≥4cm	37	12(32.43%)	25(67.57%)		
Vascular invasion				0.027	2.187(1.092–4.384)
Yes	69	30(43.48%)	39(56.52%)		
No	65	45(69.23%)	20(30.77%)		

- IHC and *in situ* immunofluorescence
- Lentiviral transduction
- ELISA
- RT-PCR
- WB analysis
- CCK8 assay
- Colony formation assay
- Transwell migration assay and transwell invasion assay
- Flow cytometry analysis
- ATP measurement
- RNA sequencing and analysis

- QUANTIFICATION AND STATISTICAL ANALYSIS

SUPPLEMENTAL INFORMATION

Supplemental information can be found online at https://doi.org/10.1016/j.isci.2024.110077.

ACKNOWLEDGMENTS

This study was supported by High-level Professional Physician Training Program of Minhang District (2020MZYS17) to H.F.; Shanghai Shenkang Hospital Development Center's Shenkang Promotion of Clinical Skills and Clinical Innovation in Municipal Hospitals Three-Year Action Plan(2020-2023) Major Clinical Research Project (Grant No. SHDC2020CR1048B) and General Program of National Natural Science Foundation of China (Grant No.82271654) to H.J.

AUTHOR CONTRIBUTIONS

H.J. and T.C. defined the research theme and guided the research experiments. H.F. performed experiments, analyzed the data and wrote the paper. All authors read and approved the final paper.

DECLARATION OF INTERESTS

No potential conflicts of interest were disclosed by the authors.

Received: August 23, 2023
Revised: November 2, 2023
Accepted: May 19, 2024
Published: May 22, 2024

REFERENCES

1. Torre, L.A., Islami, F., Siegel, R.L., Ward, E.M., and Jemal, A. (2017). Global cancer in women: Burden and trends. Cancer Epidemiol. Biomarkers Prev. *26*, 444–457. https://doi.org/10.1158/1055-9965.
2. Koh, W.J., Abu-Rustum, N.R., Bean, S., Bradley, K., Campos, S.M., Cho, K.R., Chon, H.S., Chu, C., Clark, R., Cohn, D., et al. (2019). Cervical Cancer, Version 3.2019, NCCN Clinical Practice Guidelines in Oncology. J. Natl. Compr. Cancer Netw. *17*, 64–84. https://doi.org/10.6004/jnccn.2019.0001.
3. Bhatla, N., Aoki, D., Sharma, D.N., and Sankaranarayanan, R. (2018). Cancer of the cervix uteri. Int. J. Gynaecol. Obstet. *143*, 22–36. https://doi.org/10.1002/ijgo.12611.
4. Cheng-Yen Lai, J., Lai, K.J., Yi-Yung Yu, E., Hung, S.T., Chu, C.Y., and Wang, K.L. (2018). Sentinel lymphatic mapping among women with early-stage cervical cancer: A systematic review. Taiwan. J. Obstet. Gynecol. *57*, 636–643. https://doi.org/10.1016/j.tjog.2018.08.004.
5. Li, K., Sun, H., and Guo, Q. (2019). Combinative evaluation of primary tumor and lymph nodes in predicting pelvic lymphatic metastasis in early-stage cervical cancer: A multiparametric PET-CT study. Eur. J. Radiol. *113*, 153–157. https://doi.org/10.1016/j.ejrad.2019.02.013.
6. Luo, L., Luo, Q., and Tang, L. (2020). Diagnostic value and clinical significance of MRI and CT in detecting lymph node metastasis of early cervical cancer. Oncol. Lett. *19*, 700–706. https://doi.org/10.3892/ol.2019.11180.
7. Martinez, A., Voglimacci, M., Lusque, A., Ducassou, A., Gladieff, L., Dupuis, N., Angeles, M.A., Martinez, C., Tanguy Le Gac, Y., Chantalat, E., et al. (2020). Tumour and pelvic lymph node metabolic activity on FDG-PET/CT to stratify patients for para-aortic surgical staging in locally advanced cervical cancer. Eur. J. Nucl. Med. Mol. Imag. *47*, 1252–1260. https://doi.org/10.1007/s00259-019-04659-z.
8. Woo, S., Atun, R., Ward, Z.J., Scott, A.M., Hricak, H., and Vargas, H.A. (2020). Diagnostic performance of conventional and advanced imaging modalities for assessing newly diagnosed cervical cancer: systematic review and meta-analysis. Eur. Radiol. *30*, 5560–5577. https://doi.org/10.1007/s00330-020-06909-3.
9. Wang, W., Jia, H.L., Huang, J.M., Liang, Y.C., Tan, H., Geng, H.Z., Guo, L.Y., and Yao, S.Z. (2014). Identification of biomarkers for lymph node metastasis in early-stage cervical cancer by tissue-based proteomics. Br. J. Cancer *110*, 1748–1758. https://doi.org/10.1038/bjc.2014.92.
10. Zhou, Z., Li, W., Zhang, F., and Hu, K. (2017). The value of squamous cell carcinoma antigen (SCCa) to determine the lymph nodal metastasis in cervical cancer : A meta-analysis and literature review. PLoS One *12*, e0186165. https://doi.org/10.1371/journal.pone.0186165.
11. Jono, H., and Ando, Y. (2010). Midkine: A Novel Prognostic Biomarker for Cancer. Cancers *2*, 624–641. https://doi.org/10.3390/cancers2020624.
12. Filippou, P.S., Karagiannis, G.S., and Constantinidou, A. (2020). Midkine (MDK) growth factor: a key player in cancer progression and a promising therapeutic target. Oncogene *39*, 2040–2054. https://doi.org/10.1038/s41388-019-1124-8.
13. Ito, M., Oshima, Y., Yajima, S., Suzuki, T., Nanami, T., Shiratori, F., Funahashi, K., and Shimada, H. (2019;(August 2018). Diagnostic impact of high serum midkine level in patients with gastric cancer. Ann. Gastroenterol. Surg. *3*, 195–201. https://doi.org/10.1002/ags3.12226.
14. Castaño, A., and Maurer, M.S. (2013). Evaluation of Midkine as a Diagnostic Serum Biomarker in Hepatocellular Carcinoma. Clin. Cancer Res. *19*, 3944–3954. https://doi.org/10.1158/1078-0432.CCR-12-3363.
15. Kishida, S., Mu, P., Miyakawa, S., Fujiwara, M., Abe, T., Sakamoto, K., Onishi, A., Nakamura, Y., and Kadomatsu, K. (2013). Midkine promotes neuroblastoma through Notch2 signaling. Cancer Res. *73*, 1318–1327. https://doi.org/10.1158/0008-5472.CAN-12-3070.
16. Zhao, J., Pan, Y., Li, X., Zhang, X., Xue, Y., Wang, T., Zhao, S., and Hou, Y. (2017). Dihydroartemisinin and Curcumin Synergistically Induce Apoptosis in SKOV3 Cells Via Upregulation of MiR-124 Targeting Midkine. Cell. Physiol. Biochem. *43*, 589–601. https://doi.org/10.1159/000480531.
17. Kapoor, C., Vaidya, S., Wadhwan, V., and Malik, S. (2015). Lymph node metastasis: A bearing on prognosis in squamous cell carcinoma. Indian J. Cancer *52*, 417–424. https://doi.org/10.4103/0019-509X.176750.
18. Olmeda, D., Cerezo-Wallis, D., Riveiro-Falkenbach, E., Pennacchi, P.C., Contreras-Alcalde, M., Ibarz, N., Cifdaloz, M., Catena, X., Calvo, T.G., Cañón, E., et al. (2017). Whole-body imaging of lympho-vascular niches identifies pre-metastatic roles of midkine. Nature *546*, 676–680. https://doi.org/10.1038/nature22977.
19. Tanabe, K., Matsumoto, M., Ikematsu, S., Nagase, S., Hatakeyama, A., Takano, T., Niikura, H., Ito, K., Kadomatsu, K., Hayashi, S.i., and Yaegashi, N. (2008). Midkine and its clinical significance in endometrial carcinoma. Cancer Sci. *99*, 1125–1130. https://doi.org/10.1111/j.1349-7006.2008.00796.x.
20. Moon, H.S., Park, W.I., Sung, S.H., Choi, E.A., Chung, H.W., and Woo, B.H. (2003). Immunohistochemical and quantitative competitive PCR analyses of midkine and pleiotrophin expression in cervical cancer. Gynecol. Oncol. *88*, 289–297. https://doi.org/10.1016/s0090-8258(02)00070-7.
21. Shang, C., Wang, W., Liao, Y., Chen, Y., Liu, T., Du, Q., Huang, J., Liang, Y., Liu, J., Zhao, Y., et al. (2018). LNMICC promotes nodal metastasis of cervical cancer by reprogramming fatty acid metabolism. Cancer Res. *78*, 877–890. https://doi.org/10.1158/0008-5472.CAN-17-2356.
22. Liu, S., Gao, F., Wen, L., Ouyang, M., Wang, Y., Wang, Q., Luo, L., and Jian, Z. (2017). Osteocalcin Induces Proliferation via Positive Activation of the PI3K/Akt, P38 MAPK Pathways and Promotes Differentiation Through Activation of the GPRC6A-ERK1/2 Pathway in C2C12 Myoblast Cells. Cell. Physiol. Biochem. *43*, 1100–1112. https://doi.org/10.1159/000481752.
23. Wang, Z.G., Cheng, Y., Yu, X.C., Ye, L.B., Xia, Q.H., Johnson, N.R., Wei, X., Chen, D.Q., Cao, G., Fu, X.B., et al. (2016). bFGF Protects Against Blood-Brain Barrier Damage Through Junction Protein Regulation via PI3K-Akt-Rac1 Pathway Following Traumatic Brain Injury. Mol. Neurobiol. *53*, 7298–7311. https://doi.org/10.1007/s12035-015-9583-6.
24. Mudassar, F., Shen, H., O'Neill, G., and Hau, E. (2020). Targeting tumor hypoxia and mitochondrial metabolism with anti-parasitic drugs to improve radiation response in high-grade gliomas. J. Exp. Clin. Cancer Res. *39*, 208. https://doi.org/10.1186/s13046-020-01724-6.
25. Maycotte, P., Marín-Hernández, A., Goyri-Aguirre, M., Anaya-Ruiz, M., Reyes-Leyva, J., and Cortés-Hernández, P. (2017). Mitochondrial dynamics and cancer. Tumour Biol. *39*, 1010428317698391. https://doi.org/10.1177/1010428317698391.
26. Sun, L., Wang, H., Xu, D., Yu, S., Zhang, L., and Li, X. (2022). Lapatinib induces mitochondrial dysfunction to enhance oxidative stress and ferroptosis in doxorubicin-induced cardiomyocytes via inhibition of PI3K/AKT signaling pathway. Bioengineered *13*, 48–60. https://doi.org/10.1080/21655979.2021.2004980.
27. Yang, J.Y., Deng, W., Chen, Y., Fan, W., Baldwin, K.M., Jope, R.S., Wallace, D.C., and Wang, P.H. (2013). Impaired translocation and activation of mitochondrial Akt1 mitigated mitochondrial oxidative phosphorylation Complex V activity in diabetic myocardium. J. Mol. Cell. Cardiol. *59*, 167–175. https://doi.org/10.1016/j.yjmcc.2013.02.016.
28. Deepa, S.S., Yamada, S., Zako, M., Goldberger, O., and Sugahara, K. (2004). Chondroitin sulfate chains on syndecan-1 and syndecan-4 from normal murine mammary gland epithelial cells are structurally and functionally distinct and cooperate with heparan sulfate chains to bind growth factors. A novel function to control binding of midkine, pleiotrophin, and basic fibroblast growth factor. J. Biol. Chem. *279*, 37368–37376. https://doi.org/10.1074/jbc.M403031200.
29. Yang, Y.Y., Chen, Z., Yang, X.D., Deng, R.R., Shi, L.X., Yao, L.Y., and Xiang, D.X. (2021). Piperazine ferulate prevents high-glucose-induced filtration barrier injury of glomerular endothelial cells. Exp. Ther. Med. *22*, 1175. https://doi.org/10.3892/etm.2021.10607.
30. Nathanson, S.D. (2003). Insights into the mechanisms of lymph node metastasis.

Cancer *98*, 413–423. https://doi.org/10.1002/cncr.11464.

31. Zheng, L., Liu, Q., Li, R., Chen, S., Tan, J., Li, L., Dong, X., Huang, C., Wen, T., and Liu, J. (2022). Targeting MDK Abrogates IFN-γ-Elicited Metastasis in Cancers of Various Origins. Front. Oncol. *12*, 885656–885712. https://doi.org/10.3389/fonc.2022.885656.
32. Otani, S., Fujii, T., Kukimoto, I., Yamamoto, N., Tsukamoto, T., Ichikawa, R., Nishio, E., and Iwata, A. (2019). Cytokine expression profiles in cervical mucus from patients with cervical cancer and its precursor lesions. Cytokine *120*, 210–219. https://doi.org/10.1016/j.cyto.2019.05.011.
33. Zhang, Y., Zuo, C., Liu, L., Hu, Y., Yang, B., Qiu, S., Li, Y., Cao, D., Ju, Z., Ge, J., et al. (2021). Single-cell RNA-sequencing atlas reveals an MDK-dependent immunosuppressive environment in ErbB pathway-mutated gallbladder cancer. J. Hepatol. *75*, 1128–1141. https://doi.org/10.1016/j.jhep.2021.06.023.
34. Cancer Genome Atlas Research Network, Albert Einstein College of Medicine, Analytical Biological Services, Barretos Cancer Hospital, Baylor College of Medicine, Beckman Research Institute of City of Hope, Buck Institute for Research on Aging, Canada's Michael Smith Genome Sciences Centre, Harvard Medical School, Helen F. Graham Cancer Center &Research Institute at Christiana Care Health Services, et al.. (2017). Integrated genomic and molecular characterization of cervical cancer. Nature *543*, 378–384. https://doi.org/10.1038/nature21386.
35. Krzystek-Korpacka, M., Gorska, S., Diakowska, D., Kapturkiewicz, B., Podkowik, M., Gamian, A., and Bednarz-Misa, I. (2017). Midkine is up-regulated in both cancerous and inflamed bowel, reflecting lymph node metastasis in colorectal cancer and clinical activity of ulcerative colitis. Cytokine *89*, 68–75. https://doi.org/10.1016/j.cyto.2016.09.020.
36. Tsukita, S., Furuse, M., and Itoh, M. (2001). Multifunctional strands in tight junctions. Nat. Rev. Mol. Cell Biol. *2*, 285–293. https://doi.org/10.1038/35067088.
37. Ueno, Y., Ozaki, S., Umakoshi, A., Yano, H., Choudhury, M.E., Abe, N., Sumida, Y., Kuwabara, J., Uchida, R., Islam, A., et al. (2019). Chloride intracellular channel protein 2 in cancer and non-cancer human tissues: relationship with tight junctions. Tissue Barriers *7*, 1593775. https://doi.org/10.1080/21688370.2019.1593775.
38. Cong, X., and Kong, W. (2020). Endothelial tight junctions and their regulatory signaling pathways in vascular homeostasis and disease. Cell. Signal. *66*, 109485. https://doi.org/10.1016/j.cellsig.2019.109485.
39. Laakkonen, J.P., Lappalainen, J.P., Theelen, T.L., Toivanen, P.I., Nieminen, T., Jauhiainen, S., Kaikkonen, M.U., Sluimer, J.C., and Ylä-Herttuala, S. (2017). Differential regulation of angiogenic cellular processes and claudin-5 by histamine and VEGF via PI3K-signaling, transcription factor SNAI2 and interleukin-8. Angiogenesis *20*, 109–124. https://doi.org/10.1007/s10456-016-9532-7.
40. Ham, J., Song, J., Song, G., and Lim, W. (2023). Oryzalin impairs maternal-fetal interaction during early pregnancy via ROS-mediated P38 MAPK/AKT and OXPHOS downregulation. Food Chem. Toxicol. *174*, 113665. https://doi.org/10.1016/j.fct.2023.113665.
41. Rice, G.E., Edgell, T.A., and Autelitano, D.J. (2010). Evaluation of midkine and anterior gradient 2 in a multimarker panel for the detection of ovarian cancer. J. Exp. Clin. Cancer Res. *29*, 62. https://doi.org/10.1186/1756-9966-29-62.
42. Bhatla, N., Berek, J.S., Cuello Fredes, M., Denny, L.A., Grenman, S., Karunaratne, K., Kehoe, S.T., Konishi, I., Olawaiye, A.B., Prat, J., et al. (2019). Revised FIGO staging for carcinoma of the cervix uteri. Int. J. Gynaecol. Obstet. *145*, 129–135. https://doi.org/10.1002/ijgo.12749.
43. Aynacıoğlu, A.Ş., Bilir, A., and Tuna, M.Y. (2019). Involvement of midkine in autoimmune and autoinflammatory diseases. Mod. Rheumatol. *29*, 567–571. https://doi.org/10.1080/14397595.2018.1523701.
44. Jing, X., Cui, X., Liang, H., Hao, C., and Han, C. (2017). Diagnostic accuracy of ELISA for detecting serum Midkine in cancer patients. PLoS One *12*, e0180511. https://doi.org/10.1371/journal.pone.0180511.
45. Li, Y., Fei, H., Lin, Q., Liang, F., You, Y., Li, M., Wu, M., Qu, Y., Li, P., Yuan, Y., et al. (2021). ZEB2 facilitates peritoneal metastasis by regulating the invasiveness and tumorigenesis of cancer stem-like cells in high-grade serous ovarian cancers. Oncogene *40*, 5131–5141. https://doi.org/10.1038/s41388-021-01913-3.

STAR★METHODS

KEY RESOURCES TABLE

REAGENT or RESOURCE	SOURCE	IDENTIFIER
Antibodies		
Rabbit anti-humanMDKantibody	Abcam, USA	Cat# ab236781
Mouse anti-humanBax antibody	Beyotime, China	Cat#AF0054
Rabbit anti-humanBcl-2 antibody	Beyotime, China	Cat#AF0060
Rabbit anti-humanZO-1 antibody	Affinity, USA	Cat#AF5145
Rabbit anti-humanClaudin5 antibody	Affinity, USA	Cat# AF5216
Rabbit anti-humanOccludin antibody	Affinity, USA	Cat#DF7504
Rabbit anti-human MMP9 antibody	Abcam, USA	Cat# ab76003
Rabbit anti-human MMP2 antibody	Beyotime, China	Cat# AF1420
Rabbit anti-human AKT antibody	CST, USA	Cat#9272S
Rabbit anti-human p-AKT (Ser 473) antibody	CST, USA	Cat#4058L
Rabbit anti-human p38 MAPK antibody	CST, USA	Cat#9212S
Rabbit anti-human p-p38 MAPKantibody	CST, USA	Cat#9215L
Rabbit anti-mouseLYVE-1 antibody	Abcam, USA	Cat#ab14917
Rabbit anti-GAPDH antibody	Abcam, USA	Cat# ab9485
Goat Anti-Rabbit IgG H&L (HRP)	Abcam, USA	Cat# ab6721
Goat Anti-Mouse IgG H&L (HRP)	Abcam, USA	Cat# ab6789
Chemicals, peptides, and recombinant proteins		
Recombinant Human-derived MDK Protein	MCE,USA	Cat#HY-P73295
PI3K inhibitor (LY294002)	Beyotime, China	Cat#S1737
Akt inhibitor (MK2206)	Beyotime, China	Cat#SF2712
p38 MAPK inhibitor (SB203580)	Beyotime, China	Cat#S1863
Critical commercial assays		
MDK ELISA kits	Arigo, China	Cat#ARG81533
SCCA ELISA kits	Invitrogen, USA	Cat#EH413RB
MolPure® TRIeasy™ Plus Total RNA Kit	Yeasen science, China	Cat#19211ES60
PrimeScript™ RT reagent Kit	Takara, Japan	Cat#RR037A
YF647A-Annexin V/PI Apoptosis Kit	Share-bio, China	Cat#SB-Y6026
ATP Assay Kit	Beyotime, China	Cat#S0026
JC-1 Kit	Beyotime, China	Cat#C2005
Deposited data		
RNA-seq data and clinical information for MDK	Compendia Corporation	https://www.oncomine.org/resource/login.html
Original western blot images	mendeley	https://data.mendeley.com/datasets/bgj7mhmftv/1
HLECs-MDK RNA seq	GEO	GEO:GSE263143
Experimental models: Cell lines		
C33a cells	ATCC	HTB-31
Siha cells	ATCC	HTB-35
Caski cells	ATCC	CRM-CRL-1550
Hela cells	ATCC	CRM-CCL-2
MS751 cells	ATCC	HTB-34
HLECs cells	Sciencell	2500

(*Continued on next page*)

Continued

REAGENT or RESOURCE	SOURCE	IDENTIFIER
Experimental models: Organisms/strains		
Mouse: Female nude mice	GemPharmatech Co., Ltd	Cat#D000521
Oligonucleotides		
hMDK-F, see Table S3	This paper	N/A
hMDK-R, see Table S3	This paper	N/A
hGAPDH-F, see Table S3	This paper	N/A
hGAPDH-R , see Table S3	This paper	N/A
hZO-1-F, see Table S3	This paper	N/A
hZO-1-R, see Table S3	This paper	N/A
hClaudin5-F, see Table S3	This paper	N/A
hClaudin5-R, see Table S3	This paper	N/A
hOccludin-F , see Table S3	This paper	N/A
hOccludin-R, see Table S3	This paper	N/A
Recombinant DNA		
MDK expression vector	Shanghai GeneChem Co.,Ltd	N/A
Software and algorithms		
fluorescent microscope	Leica	N/A
the Premix SYBR green PCR system	Takara, Japan	N/A
ABI Step One Plus RT-PCR machine	Applied Biosystems	N/A
Image Quant LAS 4000	GE Healthcare	N/A
flow cytometer	BD	N/A
Mikrowin 2000 software	Berthold Technologies	N/A
SPSS 23.0	IBM	N/A
GraphPad Prism 7.0	GraphPad Software	N/A
ImageJ Software	Rawak Software	N/A
Other		
DMEM/F12	HyClone	Cat#SH30004.03
ECM	Sciencell	Cat#1001
Matrigel	BD	Cat#356234
CCK8 solution	Nobleryder, China	N/A

RESOURCE AVAILABILITY

Lead contact

Further information and requests for resources and reagents should be directed to and will be fulfilled by the lead contact, Hua Jiang (jianghua@fudan.edu.cn).

Materials availability

This study did not generate new unique reagents.

Data and code availability

All data available in this study is publicly available.The RNA-seq data and clinical information for MDK were obtained from Oncomine database (https://www.oncomine.org/resource/login.html). RNA-seq data have been deposited at GEO and are publicly available as of the date of publication. Accession numbers are listed in the key resources table. Original western blot images have been deposited at Mendeley and are publicly available as of the date of publication. The DOI is listed in the key resources table. Any additional information required to reanalyze the data reported in this paper is available from the lead contact upon request.

EXPERIMENTAL MODEL AND STUDY PARTICIPANT DETAILS

Cell lines

Human cervical cancer cell lines (C33a, Siha, Caski, Hela and MS751) were obtained from American Type Culture Collection(ATCC). HLECs were obtained from Sciencell. All human cervical cancer cells were cultivated in Dulbecco's Modified Eagle Medium/Nutrient Mixture F-12(DMEM/F12, HyClone) containing 10% FBS with 5% CO_2 at 37°C. The passage numbers of the tumor cell lines do not exceed p15. HLECs were cultivated in Endothelial cell medium (ECM, Sciencell) containing 5% FBS with 5% CO_2 at 37°C. p3-p6 HLECs were used for experiments. All the cell lines were tested free of mycoplasma contamination.

Hindfoot lymphatic drainage model

Female nude mice (5 weeks old) were purchased from GemPharmatech Co., Ltd. Shanghai. China, and were randomised into two groups. There was no blind control in each group. The matrix glue was diluted 1:1 in serum-free medium for cell resuspended. MS751 MDK and MS751 NC cells (6×10^6) were injected into the mice footpad. In addition, the transplantation tumors in the footpad were surgically removed and formalin-fixed for IHC staining. Each individual experiment was performed in triplicate. The animal experiment procedure was approved by the Ethical Committee of Animal Experiments of Fudan University (202012015S).

Human studies

Paraffin sections were obtained from tissue bank of Obstetrics and Gynecology Hospital, Fudan University; 56 CSCC patients who received surgery in our hospital from 2016 to 2019 were included as CSCC group. The pathological characteristics of these patients are listed in Table 1. 12 patients who were diagnosed with hysteromyoma undergoing total hysterectomy were included as NC group. There is no statistical difference in age between two groups (51.07 ± 1.335 *vs* 45.5 ± 1.873, p=0.0696).

Serum samples were also obtained from tissue bank of Obstetrics and Gynecology Hospital, Fudan University; 140 CSCC patients who received surgery in our hospital from 2016 to 2020 and 60 healthy controls were collected. Finally, 134 CSCC (CSCC group) and 53 healthy controls (NC group) with complete clinical data and effective detection by EILSA were included. There is no statistical difference in age between the two groups (44.33 ± 5.346 *vs* 41.85 ± 8.741, p=0.0528).

All patients' diagnoses in this study were pathologically confirmed. FIGO stage was re-evaluated and staged according to the 2018 FIGO staging criteria for cervical cancer based on the patients' medical history.[42] Exclusion criteria of patients: (1) Incomplete clinical data; (2) Patients complicated with other malignant tumors, ischemic diseases, autoimmune diseases, kidney diseases, neurological diseases, inflammation, hypertension, diabetes; Studies have shown that MDK expression increases in patients with the above special status,[43,44] so exclusion criteria are included in order to eliminate research interference. (3) Patients who received preoperative treatment, such as chemotherapy, radiotherapy, immunotherapy. The proposal for this study was approved by the Institutional Review Board of Obstetrics & Gynecology Hospital, Fudan University, and granted exemption from informed consent (2020-165).

METHOD DETAILS

IHC and *in situ* immunofluorescence

Experiments were performed as previously described.[45] Cells cultured on chamber slides were fixed with 4% paraformaldehyde for 20mins and permeabilized in 0.1% TritonX-100 for 10mins. Murine anti-human antibodies were added to the slides and incubated overnight at 4°C. The corresponding fluorescent secondary antibody was added and incubated at 4°C for 1h. For mitochondrial membrane potential detection, HLECs were stained with JC-1 for 20mins according to the manufacturer's instructions (Beyotime, Shanghai, China). The fluorescence of JC-1 red represented multimeric form, and JC-1 green represented monomeric form. Mitochondrial membrane potential as the ratio of JC-1 red to JC-1 green was detected by immunofluorescence. The fluorescence images were investigated under a fluorescent microscope (Leica Micro systems, Wetzlar, Germany) with DAPI co-staining. Quantification of images was determined by Image J software, to calculate the mean fluorescence intensity (MFI) per field.

Paraffin sections were dewaxed using gradient alcohol. Ten millimolar preheated citric acid/citrate repair buffer (pH6) and 3% H_2O_2 were used to repair antigens and block non-specific peroxidase activity. The slides were incubated with antibodies at 4°C overnight. The information of antibodies was listed in Table S2. Secondary antibody was subsequently incubated for 30mins, and DAB mixed substrate was used for detection using optical microscope. Protein expression was scored by two independent observers according to previously published methodology.[45] A scoring system defined as signalling intensity(A) × the percentage of positive cells(B) was used to quantify the protein expression. 0,1,2,3 in(A) represented no staining, weak staining and strong staining, and 0-3 in (B) represented 0%, 1-25%, 25-50% and >50% positively stained cells. Final scores of 1-3 indicated low(negative).

Lentiviral transduction

Three oligo sequences of the MDK-specific shRNA (shMDK) duplex were 5′- cgACTGCAAGTACAAGTTTGA-3′, 5′-caAGACCAAAG CAAAGGCCAA-3′ and 5′-gcGCTACAATGCTCAGTGCCA-3′, respectively. Lentiviral vectors encoding short hairpin RNAs were generated by inserting shMDK into the hU6-MCS-Ubiquitin-EGFP-IRES-puromycin vector (GeneChem Inc, Shanghai, China). The empty plasmid (NC) was used as a control. Cell lines stably expressing MDK shRNA were generated by infection of lentivirus, which was produced by HEK293T cells using envelope plasmid pMD2.G and packaging plasmid psPAX2. Human MDK cDNA was cloned into the

Ubi-MCS-3FLAG-CBh-gcGFP-IRES-puromycin vectors. The primer sequences were forward, 5′-GGGTCAATATGTAATTTTCAGTG-3′, and reverse, 5′-CCTTATAGTCCTTATCATCGTC-3′. Cell lines stably expressing MDK cDNA were generated by infection of lentivirus, which was produced by HEK293T cells using envelope plasmid pMD2.G and packaging plasmid psPAX2. Briefly, the cells were infected with the indicated virus for 24h. Then, the virus was removed and the cells were selected with puromycin. After 2 weeks, the proportion of GFP fluorescence positive cells was detected by flow cytometry to evaluate the efficiency of lentiviral transduction. More than 85% of GFP fluorescent positive cells represented effective transfection (Datas are not shown), and the cells were used in follow-up experiments.

ELISA

Serum samples were thawed on ice and used to detect the levels of s-MDK and s-SCCA by ELISA. MDK ELISA kits (Arigo, China) and SCCA ELISA kits (Invitrogen, USA) were used. All operations were performed follow the manufacturer's instruction. No reagent was added to the blank control well.

RT-PCR

Total RNA was extracted using RNA-Quick Purification Kit (Yeasen science, Shanghai, China) and reverse transcribed into cDNA using the PrimeScript Reverse Transcription Kit (Takara, Japan). RT-PCR was subsequently performed in triplicate using the Premix SYBR green PCR system (Takara, Japan) and appropriate primers on an ABI Step One Plus RT-PCR machine (Applied Biosystems, Calif, USA). GAPDH was used as the internal control. The relative mRNA levels were analyzed using the $2-\Delta\Delta Ct$ method. The oligonucleotide primers are listed in Table S3. The cycling conditions employed for RT-PCR are shown in Table S4.

WB analysis

The protein was resolved by 10% SDS-PAGE and then electro blotted onto PVDF membranes, which were treated sequentially in 5% nonfat milk and then incubated with primary antibodies overnight at 4°C and secondary antibodies for 1h at room temperature. After incubation with enhanced chemiluminescence reagents, the membranes were visualized under an Image Quant LAS 4000 (GE Healthcare, Calif, USA). The information of antibodies was listed in Table S2. GAPDH was used as the internal control.

CCK8 assay

Cells were seeded at appropriate cell density (cervical cancer cells 5.0×10^3 cells/well; HLECs 2.0×10^3 cells/well) in 96-well culture plate. Ten microliter CCK8 solution (Nobleryder, Beijing, China) was added into each well at 0, 24, 48 and 96h. After incubation for a certain time (cervical cancer cells 1h; HLECs 3h), OD values in each well at the wave length of 450 nm were measured using a microplate reader. Each assay was repeated at least three times.

Colony formation assay

Two thousand cells/well were seeded in a six-well plate at 37°C for 10 days with 4ml medium/well. The attached cells were fixed and subjected to 1% crystal violet staining. Colonies consisting of at least 50 cells were detected using ImageJ Software (Rawak Software, Germany).[45]

Transwell migration assay and transwell invasion assay

Six hundred microliter DMEM/F12 containing 10% FBS was placed into a 24-well culture plate in advance. Cells were incubated with 200μl serum-free medium in a transwell chamber on the top of the well. For transwell invasion assay, sixty microliter of Matrigel (BD, New Jersey, USA) at a 1:8 dilution was coated and solidified on a transwell membrane with 8μm pores (Corning Costar, New York, USA) at 37°C for 5h. After incubation for 24-36h at 37°C, the membranes were fixed with methanol for 10mins and stained with 0.1% crystal violet for 15mins. The number of migrated/invasive cells of five random fields were visualised and counted under a Leica inverted phase contrast microscope. Each individual experiment was performed in triplicate.

Flow cytometry analysis

For apoptosis analysis, YF647A-Annexin V and PI Apoptosis Kit (Share-bio, Shanghai, China) was used following the manufacturer's instructions. We took the total proportion of annexin V-positive cells (quadrants II and III) as the apoptotic rate, regardless of the PI status. FACS analysis was performed on a flow cytometer (BD, New Jersey, USA), and data analysis was performed using FlowJo Software.

For the analysis of intracellular markers (active caspase-3), cells were trypsinised into a single cell suspension, permeabilized, incubated for 20mins with murine anti-human active caspase-3(1:50, BD, New Jersey, USA).

ATP measurement

Extracellular ATP in cell-free medium supernatant was quantified using ATP Assay Kit (Beyotime, China) according to the manufacturer's instructions, and the luminescence produced was measured (Mithras, Mikrowin 2000 software, Berthold Technologies, Thoiry, France).

RNA sequencing and analysis

Total RNA was extracted from cells using Trizol reagent. Agilent 2100 BioAnalyzer was used to detect RNA integrity. The mRNA with poly-A tail was enriched by Oligo(dT) magnetic beads. In NEB Fragmentation Buffer, divalent cations were used to randomly interrupt the mRNA, and the library was constructed in accordance with the common NEB library construction method. The mRNA fragment was reversely transcribed into cDNA, and the double-stranded cDNA was purified. Then, the end repair was performed, A-tail was added, and the sequencing adapters was connected. The 250-300bp cDNA was screened with magnetic beads for PCR amplification, then the PCR products were purified with magnetic beads, and finally the library was obtained.

Differential expression analysis of two groups (three biological replicates per condition) was performed using the DESeq2 R package (1.20.0). DESeq2 provide statistical routines for determining differential expression in digital gene expression data using a model based on the negative binomial distribution. Genes with p-value less than 0.05 & |log2FoldChange|>0.0 found by DESeq2 were assigned as differentially expressed.

Gene Ontology (GO) enrichment analysis of differentially expressed genes was implemented by the cluster Profiler R package, in which gene length bias was corrected. GO terms with corrected p-value less than 0.05 were considered significantly enriched by differential expressed genes. KEGG is a database resource for understanding high-level functions and utilities of the biological system, such as the cell, the organism and the ecosystem, from molecular-level information, especially large-scale molecular datasets generated by genome sequencing and other high-through put experimental technologies (http://www.genome.jp/kegg/). We conducted KEGG enrichment analysis on differentially expressed genes using the clusterProfiler package, with a corrected p-value less than 0.05 considered as the level of statistical significance.

QUANTIFICATION AND STATISTICAL ANALYSIS

Statistical analysis was performed with SPSS 23.0 (IBM, USA) and GraphPad Prism 7.0 (GraphPad Software, USA). For the cellular data, the significance of the difference in the mean value was determined using a two-tailed Student's t test. The results are presented as the mean $\pm$ SD of at least three independent experiments. Since the concentrations of s-MDK and s-SCCA were not normally distributed, Mann-Whitney U test was used to analyze the difference of s-MDK or s-SCCA expression between the two groups. The results are presented as median (25%,75%). Logistic regression test was conducted to assess the association between MDK and pathological parameters. ROC curves were applied to evaluate the diagnostic efficacy of s-MDK and s-SCCA in terms of LNM. $p<0.05$ was considered statistically significant.